Nuclear Instruments and Methods in Physics Research B 267 (2009) 3050–3054

Contents lists available at ScienceDirect

Nuclear Instruments and Methods in Physics Research B

journal homepage: www.elsevier.com/locate/nimb

Electronic effects in radiation damage simulations

D.M. Duffy [a,b,*], S. Khakshouri [a], A.M. Rutherford [a]

[a] London Centre for Nanotechnology, Dept. of Physics and Astronomy, University College London, Gower Street, London, WC1E 6BT, UK
[b] EURATOM/UKAEA Fusion Association, Culham Science Centre, Oxfordshire, OX14 3DB, UK

ARTICLE INFO

Article history:
Available online 16 June 2009

PACS:
61.80.Az
61.80.Jh
61.82.Bg
63.20.kd
89.30.Jj

Keywords:
Radiation damage
Iron
Tungsten
Electronic stopping
Electron–phonon coupling
Molecular dynamics

ABSTRACT

A methodology for including electronic effects in classical radiation damage simulations is presented. The method is used to calculate the number of residual defects for low energy (10 keV) cascades in Fe, as a function of the electron–phonon coupling strength. It was found that strong electron–phonon coupling reduced the number of residual defects by rapidly removing energy from the cascade and reducing the thermal spike. Intermediate coupling increased the number of defects by quenching the thermal spike and reducing defect recombination. Thermostatting the cascade with the local, time dependent electronic temperature, rather than the ambient temperature, reduced the number of residual defects by enhancing defect recombination. Swift heavy ion irradiation in tungsten was modeled using the same methodology. In this case we found that the number of residual defects created by a given electronic stopping power was strongly dependent on the temperature variation of the electronic heat capacity. In contrast to cascade simulations, the interstitials were located closer to the core of the ion track than the vacancies.

1. Introduction

Structural modification of materials by radiation is relevant to a broad range of technologically relevant processes, including the design of nuclear power plants and the nanostructuring of materials. Models of these radiation effects could play a major role in the understanding and control of such processes, but accurate predictive models are currently restricted to a limited number of applications. For example, low energy particle irradiation can be modeled successfully using cascade simulations in materials for which there are reliable interatomic potentials.

Models of radiation events which result in significant electronic excitation, such as laser irradiation, swift heavy ion irradiation and fusion neutrons, offer additional challenges to those presented by low energy particle irradiation. The inelastic energy loss due to electronic stopping has been included in cascade simulations by introducing a friction term in the equations of motion [1,2], but the effect of the deposited energy on subsequent lattice evolution was neglected. Laser and swift heavy ion irradiation deposit energy primarily in the electronic system and the lattice and electrons remain out of equilibrium for a timescale of the order of a few picoseconds. Femtosecond laser experiments are often interpreted using the two temperature model [3], which describes the temporal and spatial evolution of the electronic and lattice temperatures by coupled thermal transport equations [4]. Two temperature models do not, however, give information about structural modifications, therefore several groups have coupled such models to molecular dynamics simulations to give what is known as 2TM-MD hybrid models. The idea behind such models is that the electronic temperature evolution is calculated from numerical solutions of diffusion equations and energy is exchanged between the electronic model and the atomistic model of the lattice. Models of this kind have been used to simulate low energy cascades and laser ablation [5–7].

We have recently developed a 2TM-MD model that can be used simulate a range of radiation environments, by imposing different initial conditions [8]. Energy lost by the atomic system, by inelastic electronic scattering and electron–phonon coupling, is deposited in the electronic system, where it diffuses and re-deposits energy to the lattice. Thus the electronic system acts as a means for energy transport and storage. Low energy cascades are simulated by standard procedures but the energy lost to the electrons is gained by the electronic system [9]. The effect of swift heavy ion radiation is modeled by initializing the simulation with a column of "hot" electrons [10]. Intermediate radiation energies can be simulated

* Corresponding author. Address: London Centre for Nanotechnology, Dept. of Physics and Astronomy, University College London, Gower Street, London, WC1E 6BT, UK.
E-mail address: d.duffy@ucl.ac.uk (D.M. Duffy).

0168-583X/$ - see front matter © 2009 Elsevier B.V. All rights reserved.
doi:10.1016/j.nimb.2009.06.047

by a combination of a cascade and a column of hot electrons. Thus the synergy between displacement damage and electronic effects can be captured [11].

The model improves traditional cascade simulations in metals, in that it includes a method for removing excess energy from the simulation cell which depends on the thermal properties. The number of stable defects created by a radiation event depends critically on the rate of cooling of the thermal spike; therefore a realistic representation of the cooling process is vital for accurate damage prediction. Whilst classical molecular dynamics simulations give a good description lattice thermal conductivity, at least above the Debye temperature, metallic thermal conductivity is dominated by electronic transport and is poorly described by MD simulations. The methodology we have developed introduces a mechanism whereby energy transferred to the electrons, via inelastic scattering or electron–phonon coupling, can be transported from the simulation cell by electronic thermal conductivity.

2. Methodology

The methodology is explained in detail in earlier papers [8,10]. The basic concept is that the trajectories of the atoms are calculated by standard molecular dynamics (MD), using the DL_POLY code [12], and the spatial and temporal evolution of the electronic temperature is calculated using a finite difference solution of the heat diffusion equation. At each time step energy is exchanged between the atomic and electronic systems in such a way that energy is conserved locally, and the amount of energy exchange depends on the local temperature difference between the electronic and atomic systems. A cubic grid is superimposed on the atomistic MD simulation cell and the electronic temperature is defined on this grid. The cells are referred to as coarse-grained electronic temperature cells and each contains a few hundred atoms. The electronic temperature grid extends well beyond the atomistic simulation cell and the outer cells are kept at a constant temperature, to represent the temperature of the "rest of the system".

Following Caro and Victoria [13], we employ a Langevin thermostat to implement energy exchange between the electronic and atomic subsystems. We consider two mechanisms for energy exchange with the electrons, electron–phonon coupling and electronic stopping. Electronic stopping is included as a friction term, which is implemented for atoms above some critical velocity (v_c). Electron–phonon coupling is also included as a friction term but, as it is a two-way energy exchange, there is an additional term representing energy input to the lattice from the electrons, and this takes the form of a random force with characteristics determined by the fluctuation dissipation theorem. Therefore the atomic equations of motion are given by:

$$m\frac{\partial \mathbf{v}_i}{\partial t} = \mathbf{F}_i(t) - (\gamma_p + \gamma_s)\mathbf{v}_i + \widetilde{\mathbf{F}}(t). \tag{1}$$

Here $\mathbf{v}_i$ and m are the velocity and mass of atom i and $\underline{\mathbf{F}}_i(t)$ is the force acting on atom i due to the interaction with the surrounding atoms at time t. The friction terms, with coefficients γ_p and γ_s, represent energy loss to the electronic system by electron–phonon coupling and electronic stopping, respectively. The stochastic force $\widetilde{\mathbf{F}}(t)$ returns energy to the atoms, from the electronic system, by electron–phonon coupling. The mean value of the force is zero and the magnitude of the fluctuations is related to the local electronic temperature (T_e) by the fluctuation dissipation theorem

$$\left\langle \widetilde{\mathbf{F}}(t') \cdot \widetilde{\mathbf{F}}(t) \right\rangle = 2k_B T_e \gamma_p \delta(t' - t). \tag{2}$$

The spatial and temporal evolution of the electronic temperature is calculated by a finite difference solution of the heat diffusion equation:

$$C_e\frac{\partial T_e}{\partial t} = \nabla(\kappa_e \nabla T_e) - g_p T_e + g_p T_a + g_s T'_a. \tag{3}$$

Here C_e and κ_e are the electronic specific heat and electronic thermal conductivity respectively, g_p and g_s are coupling constants for energy exchange between the atomic and electronic systems. T_a is related to the average kinetic energy of the atoms in a coarse-grained cell and T'_a is related to the average kinetic energy of the subset of atoms with energy greater than v_c. Here energy is lost to the lattice by term 2 on the right hand side of (3) and gained from the lattice by terms 3 and 4. Energy conservation is imposed by relating the parameters (g_p, g_s, T_a and T'_a) to the parameters of the MD simulation (m, $\underline{v}_i$ and γ_p and γ_s) as outlined in [8].

The simulation setup depends on the type of radiation to be modeled. For low energy cascades we impose periodic boundary conditions on the atomistic simulation cell and constant temperature boundary conditions on the boundary of the extended electronic temperature cell. The cascade is initiated in the centre of the atomistic cell. Energy lost by the atomistic system, due the friction term in the equation of motion, is input as a source term in the electronic heat diffusion equation. The temperature associated with stochastic force in (2) refers to the local electronic temperature, which varies in time and space. For this reason we refer to it as an inhomogeneous Langevin thermostat.

Swift heavy ion irradiation can be modeled using the same methodology. Here we assume that the ion has passed through the simulation cell leaving a track of excited electrons in its wake. We assume that after a few femtoseconds the highly excited electrons will have experienced sufficient collisions to establish an approximate Fermi Dirac distribution, associated with a local electronic temperature. We calculate the excited electronic temperature (T_x) in the track from the initial electronic temperature (T_0), the electronic stopping power (S, the energy loss per unit distance), the cross-section area of the track (A) and the temperature dependant electronic heat capacity (C_e). If we assume that the energy is initially deposited in the central column of coarse-grained cells (cross-section area, A), the electronic temperature (T_x) is calculated using the following equation:

$$S/A = \int_{T_0}^{T_x} C_e(T'_e)\,dT'_e. \tag{4}$$

Constant temperature boundary conditions are imposed in the electronic simulation cell in the two directions perpendicular to the track and periodic boundary conditions are used in the direction parallel to the track. The electronic energy diffuses and deposits energy in the lattice, resulting in heating and, in some cases, local melting.

The model requires a number of material parameters, such as the electronic heat capacity, the electronic thermal conductivity, the electron–phonon coupling constant and electronic stopping parameter. Each parameter will depend on the electronic temperature as discussed for a range of metals by Lin et al. [14,15]. For results presented in this paper we have used the experimental room temperature thermal conductivity for both Fe ($80\ \mathrm{Wm^{-1}\,K^{-1}}$) and W ($177\ \mathrm{Wm^{-1}\,K^{-1}}$). We use a form of the specific heat capacity for Fe that varies linearly with temperature at low temperature and saturates at $3k_b$/atom (k_b is Boltzmann's constant) at high temperature. We compare the results for two heat capacity models for W as discussed below. A range of electron–phonon coupling constants is used for the Fe simulations and a typical experimental value is used for W.

3. Results and discussion

We present the results from two types of simulations in this paper, which represent extensions of work presented previously. The

first are results from low energy (10 keV) cascade simulations in Fe and the second are results of swift heavy ion simulations in W, where we investigate the role of the electronic heat capacity in electronic energy storage and transport. The two types of simulation represent the extremes of the full range of radiation types, where the energy is deposited predominantly in the atomic system for low energy radiation and in the electronic system for very high energy, heavy ion radiation. We have chosen to model tungsten for the high energy irradiation because there are detailed calculations of the temperature dependence of the specific heat in this material and because of its high resistance to radiation damage.

3.1. Cascade simulations

We have used the methodology presented above to study the effect of the electron–phonon coupling strength on the residual defect damage created by low energy (10 keV) cascades. A cubic simulation cell with 250,000 Fe atoms ($50 \times 50 \times 50$ unit cells) was created and this was subdivided into $9 \times 9 \times 9$ coarse-grained cells, each corresponding to 343 atoms. The coarse-grained grid was extended to a cubic grid with 100 coarse-grained cells per side, for the electronic thermal diffusion solution. A variable time step was used for the simulations. The Dudarev–Derlet potential is used for the Fe interactions [16].

Two sets of simulations were performed. One used a standard Langevin thermostat with a constant thermostatting temperature (300 K), which corresponds to a material with very high (infinite) thermal diffusivity. Thus any energy lost to the electronic system is rapidly transported away from the simulation cell and the electronic system is acts as a heat sink. The second set of simulations employed the method discussed above, where the lattice is thermostatted to the *local* electronic temperature. The electronic temperature is calculated from the finite difference solution to the heat diffusion equation and therefore it depends strongly on the thermal properties of the metal. In this case the electronic system provides a mechanism for energy storage and redistribution [17]. Each simulation was repeated for four distinct primary knock-on atom (PKA) directions.

The numbers of residual defects for the two sets of simulations are plotted against the electron–phonon coupling strength in Fig. 1. Note that, unlike the results presented in [9], we have removed the effect of electronic stopping in these simulations by setting γ_s equal to zero. Thus the difference between the two curves in figure Fig. 1 arises exclusively from thermostatting the atomistic simulation with the *local* electronic temperature in one case (inhomogeneous) and a constant 300 K in the second (homogeneous) case. The local

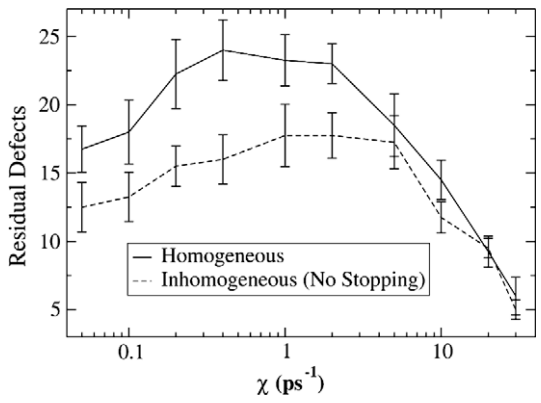

Fig. 1. The mean number of residual defects for 10 keV cascade simulations in Fe calculated using the homogeneous and inhomogeneous thermostats, plotted as a function of the electron phonon coupling strength.

electronic temperature is controlled by the thermal properties (heat capacity and thermal conductivity) of the metal.

The results show two strong features. Firstly there is a non-monotonic relationship between the electron–phonon coupling strength and the residual defect concentration, which is particularly strong for the homogeneous thermostat. This can be explained as follows. For strong electron–phonon coupling the large friction term acts to remove energy rapidly from the simulation, effectively damping the formation of the thermal spike. Thus the full disordered region does not form. Very weak electron–phonon coupling results in residual defect numbers approaching those found in constant energy (NVE) simulations (15.5 ± 1.5). For intermediate coupling constants the full thermal spike forms but the rate that energy is removed from the cascade, by electron–phonon coupling, tends to quench the disorder, resulting in an increase in the residual defect concentration compared to low coupling simulations. The inhomogeneous simulations, where the local electronic temperature is used as the thermostatting temperature, show a similar non-monotonic trend. However it has a lower number of residual defects than the corresponding homogeneous thermostat, for each of the electron–phonon coupling constants. The reduced defect concentration is caused by slower cooling due to energy storage in the electrons. The electronic system effectively acts as a heat bath, re-depositing energy into the lattice and increasing the defect recombination rate.

3.2. Ion track simulation in W

Swift heavy ion irradiation deposits energy primarily in the electronic system and we can use the current model to simulate such very high energy radiation by initialising the simulation with a locally elevated electronic temperature. In an earlier publication we demonstrated that such effects could result in permanent damage, in the form of interstitial clusters and vacancies, concentrated within a few nanometres of the path of the ion [10]. Here we investigate how the temperature dependence of the electronic heat capacity affects the radiation damage. A high electronic heat capacity leads to a low electronic diffusivity, so that energy from a radiation event will be slower to diffuse away. This can lead to more damage, as more energy gets transferred to the lattice before diffusing away. Energy storage in the electronic subsystem may have important consequences, not only in terms of the initial damage caused by irradiation, but also for annealing of defects created by radiation. It has been observed that metals with higher electronic heat capacity are more susceptible to annealing of defects on irradiation [10]. At low temperatures, the Sommerfeld expansion gives the widely used result that the electronic heat capacity is linear in temperature ($C_e = \gamma T$). Values for the coefficient γ are generally measured experimentally under equilibrium conditions. Electronic excitation can cause electron temperatures to be orders of magnitude higher than the lattice temperature. Lin, Zhigilei and Celli have pointed out that, under such non-equilibrium conditions, there may be large deviations in C_e from this linear behaviour [14,15]. With the use of electronic structure calculations, taking into account the detailed structure of the electronic density of states, they found that for some classes of metals the low temperature approximation leads to an overestimate of C_e, while for others it leads to an underestimate.

In order to investigate the effect of the temperature dependence of electronic specific heat on radiation damage, we used two different models for $C_e(T_e)$. The first C_{exp}, reproduces the experimentally observed linear behaviour at low temperatures [18] $C_{exp} = \gamma_{exp} T_e$. The second C_{Lin}, is the electronic specific heat obtained from electronic structure calculations by Lin et al. [15] up to 17,050 K, and a constant C_{max} for temperatures above this. In order to make the comparison balanced, the first model was taken to saturate to

the same value (C_{max}) at high temperatures as the C_{Lin}, by defining $C_{exp} = C_{max} \tanh(\gamma_{exp} T_e / C_{max})$. Fig. 2 shows the two models for the specific heat for comparison. It can be seen that extrapolation of the experimental curve to high temperatures underestimates C_e over a large temperature range.

The difference between the two models has a considerable effect on the evolution of the electronic and lattice temperatures. The initial electron temperatures in the excited region, T_x, calculated from Eq. (4), for an electronic stopping power of 35 keV/nm, are 2.42×10^5 K and 2.32×10^5 K for C_{exp} and C_{Lin} respectively. A cubic simulation cell with 986,078 atoms was used and the W atoms interacted via the Finnis–Sinclair potential [19]. The size of the coarse-grained cells was 2.78 nm. The initially excited region of electrons consists of a column of coarse-grained cells running through the middle of the simulation cell.

Fig. 3 shows the lattice and electron temperatures at the centre of the simulation cell (where the electrons are initially excited) as a function of time. At the earliest times (not seen in Fig. 2), T_e is higher for the Lin model because of the higher T_x value. This difference vanishes during the first 50 fs, as the electronic temperatures rapidly cool. The electronic diffusivity in the C_{exp} model then begins to increase as the specific heat decreases. The lower specific heat C_{exp} leads to faster diffusion of energy out of the excited region. This difference dominates over the higher initial temperature, resulting in more lattice heating and melting for the Lin model.

Fig. 4 shows the number of defects in the simulation cell as a function of time. The higher electronic heat capacity (C_{Lin}) leads to slower cooling of the excited electrons. This gives rise to the creation of more defects in the system, and a higher number of residual defects are left after the system has re-equilibrated. The slower rate of cooling of the excited electrons leads to a longer defect creation period, as well as a longer defect annealing period. The peak number of defects created with the Lin model heat capacity is nearly six times higher than for the C_{exp} model, with approximately 1.6 more defects remaining at the end of the simulation.

The distribution of residual defects created after an ion track simulation, displays vacant sites further from the excited core than interstitial atoms. This is in contrast to displacement cascades, where interstitials are transported away from the core efficiently via replacement collision sequences, leaving a vacancy rich core. Plots of the radial distribution of vacancies and interstitials at various times (see Fig. 5), reveal a shock wave propagating from the core, with interstitial atoms initially pushed out of their lattice sites to larger radii. While most of this damage at larger radii begins to anneal after approximately 3 ps, the damage at small radii persists. Interstitial atoms on the periphery of the core migrate into the core as the lattice contracts. A proportion of these are unable to recombine with vacancies so the interstitials are effectively quenched in at small radii, producing an interstitial rich core.

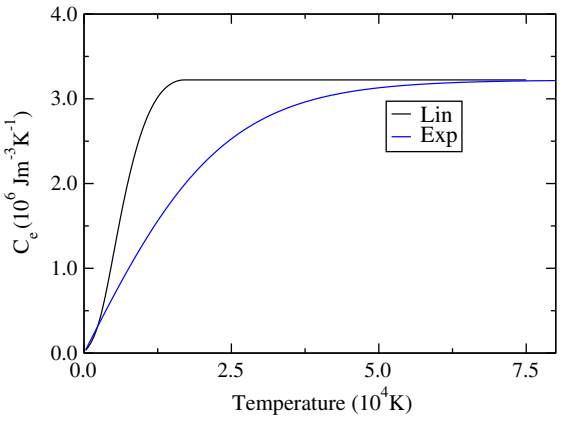

Fig. 2. Two models for the temperature dependence of the electronic specific heat capacity.

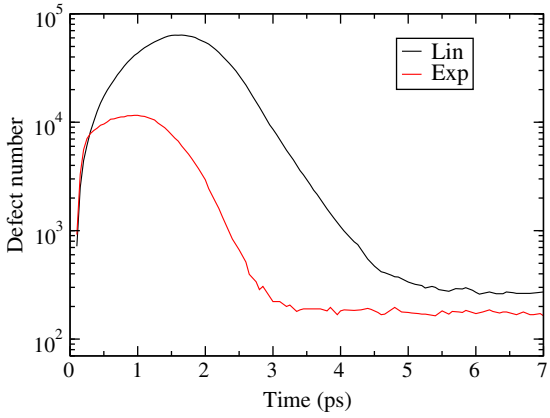

Fig. 4. The time evolution of the number of defects for the two models of the electronic heat capacity.

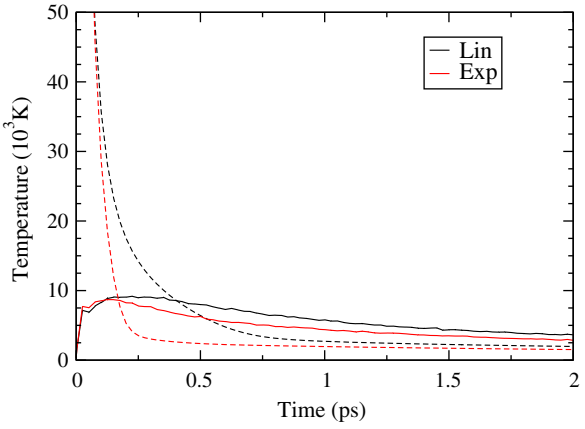

Fig. 3. The time evolution of the electronic temperature (broken line) and the lattice temperature (solid line) for the central column of the simulation cell.

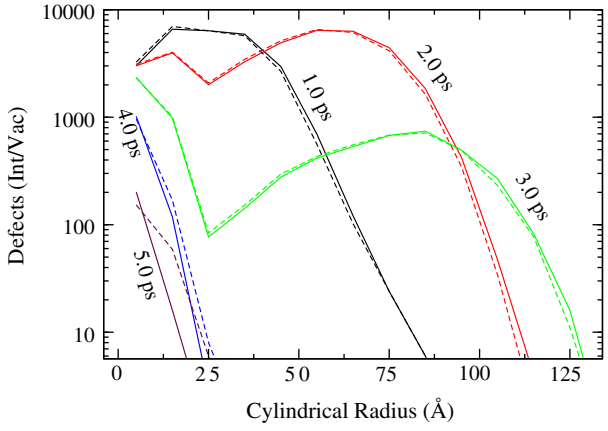

Fig. 5. The number of defects as a function of distance from the centre of the ion track for a range of simulation times. Interstitiitials are shown as sold lines and vacancies as dashed lines.

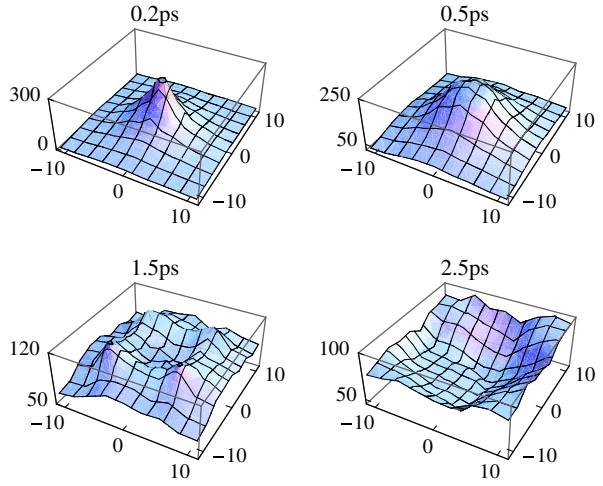

Fig. 6. Cross-section perpendicular to the ion track axis of the local pressure in coarse-grained temperature cells at various times. The *x*- and *y*-axes are position coordinates in nm. The *z*-axis is the pressure in katms.

A plot of the local pressure in the coarse-grained cells of our model (Fig. 6) shows an initially sharp peak of high pressure in the excited region, which rapidly broadens and decreases in height. At later times, the pressure is lower in the middle of the simulation cell, which leads to contraction of the lattice in this region. This lattice contraction may be responsible for pushing the interstitials into the core of the ion track.

4. Conclusions

We have described a methodology for including electronic effects in radiation damage simulations for metals that models energy storage and redistribution by the electronic system. The methodology includes a consistent way for removing the excess energy in cascade simulations of radiation that accurately reflects the metallic thermal conductivity. It has been used to model damage caused by particle irradiation at both the low (10 keV) and very high (several MeV) energy extremes of the radiation spectrum. The electronic effects depend strongly on the material parameters, such as the electron–phonon coupling strength, the thermal conductivity and the electronic heat capacity.

The residual damage resulting from low energy cascades was found to have a non-monotonic dependence on the electron–phonon coupling strength. Strong electron–phonon coupling rapidly removes energy from the cascade and inhibits the formation of the full thermal spike, thus the number of residual defects is lower than the low coupling case. The full thermal spike develops in simulations with intermediate coupling strength but the electron–phonon coupling cools the spike and reduces defect annealing. Thus for intermediate coupling strengths a higher number of residual defects is created than is found in the low coupling case.

An accurate description of the temperature dependence of the electronic heat capacity was found to be necessary for the simulation for swift heavy ion irradiation, due to the highly elevated electronic temperature. The heat capacity plays two significant roles. It determines the elevated electronic temperature reached for a given electronic stopping power and it affects the electronic diffusivity. A significant difference was found in the residual defects numbers for tungsten when using than accurate model for the specific heat and using a simple model extrapolated from the low temperature experimental heat capacity.

In summary, the method outlined in the paper provides us with a scheme for including energy exchange between the electrons and the lattice, electronic energy storage and electronic energy transport in MD simulations. The methodology can be used to model damage for a range of radiation environments.

Acknowledgements

We acknowledge support of United Kingdom Engineering and Sciences Research Council and the European Communities under the contract of Association between EURATOM and UKAEA. Computer resources on HPC*x* were provided via our membership of the UK's HPC Materials Chemistry Consortium and funded by EPSRC.

References

[1] K. Nordlund, M. Ghaly, R.S. Averback, M. Caturla, T.D. de la Rubia, J. Tarus Phys. Rev. B 57 (1998) 556.
[2] K. Nordlund, L. Wei, Y. Zhong, R.S. Averback, Phys. Rev. B 57 (1998) R13965.
[3] M.I. Kaganov, I.M. Lifshitz, L.V. Tanatorov, Sov. Phys. JETP 4 (1957) 173.
[4] R.H.L. Groeneveld, R. Sprik, A. Lagendijk, Phys. Rev. B 51 (1995) 11433.
[5] A. Duvenbeck, A. Wucher, Phys. Rev. B 72 (2005) 165408.
[6] C. Schafer, H.M. Urbassek, L.V. Zhigilei, Phys. Rev. B 66 (2002) 115404.
[7] D.S. Ivanov, L.V. Zhigilei, Phys. Rev. B 68 (2003) 064114.
[8] D.M. Duffy, A.M. Rutherford, J. Phys.: Condens. Mat. 19 (2007) 016207.
[9] A.M. Rutherford, D.M. Duffy, J. Phys.: Condens. Mat. 19 (2007) 496201.
[10] D.M. Duffy, N. Itoh, A.M. Rutherford, A.M. Stoneham, J. Phys.: Condens. Mat. 20 (2008) 082201.
[11] D.M. Duffy, A.M. Rutherford, J. Nucl. Mat. 36 (2009) 19.
[12] W. Smith, T. Forester, J. Mol. Graphics 14 (1996) 135.
[13] A. Caro, M. Victoria, Phys. Rev. A 40 (1989) 2287.
[14] Z.V. Lin, L.V. Zhigilei, Appl. Surf. Sci. 253 (2007) 6395.
[15] Z.V. Lin, L.V. Zhigilei, V. Celli, Phys. Rev. B. 77 (2008) 214108.
[16] S.L. Dudarev, P.M. Derlet, J. Phys.: Condens. Mat. 17 (2005) 7097.
[17] A.M. Stoneham, Nucl. Instr. and Meth. B 48 (1990) 389.
[18] C. Kittel, Solid State Physics, John Wiley, New York, 1996.
[19] M.W. Finnis, J.E. Sinclair, Philos. Mag. A 50 (1984) 45.